Organic & Biomolecular Chemistry

ARTICLE

Cellular localisation of structurally diverse diphenylacetylene fluorophores

David R. Chisholm,[†a,d*] Joshua G. Hughes,[†a,b,f] Thomas S. Blacker,[c] Rachel Humann,[d,e] Candace Adams,[a] Daniel Callaghan,[a] Alba Pujol,[a] Nicola K. Lembicz,[e] Angus J. Bain,[c] John M. Girkin,[f*] Carrie A. Ambler[a,b*] and Andrew Whiting[a,d*]

Fluorescent probes are increasingly used as reporter molecules in a wide variety of biophysical experiments, but when designing new compounds it can often be difficult to anticipate the effect that changing chemical structure can have on cellular localisation and fluorescence behaviour. To provide further chemical rationale for probe design, a series of donor-acceptor diphenylacetylene fluorophores with varying lipophilicities and structures were synthesised and analysed in human epidermal cells using a range of cellular imaging techniques. These experiments showed that, within this family, the greatest determinants of cellular localisation were overall lipophilicity and the presence of ionisable groups. Indeed, compounds with high LogD values (>5) were found to localise in lipid droplets, but conversion of their ester acceptor groups to the corresponding carboxylic acids caused a pronounced shift to localisation in the endoplasmic reticulum. Mildly lipophilic compounds (LogD = 2-3) with strongly basic amine groups were shown to be confined to lysosomes i.e. an acidic cellular compartment, but sequestering this positively charged motif as an amide resulted in a significant change to cytoplasmic and membrane localisation. Finally, specific organelles including the mitochondria could be targeted by incorporating groups such as a triphenylphosphonium moiety. Taken together, this account illustrates a range of guiding principles that can inform the design of other fluorescent molecules but, moreover, has demonstrated that many of these diphenylacetylenes have significant utility as probes in a range of cellular imaging studies.

Introduction

The design and synthesis of new fluorescent molecules for cellular imaging purposes has become a rich and burgeoning field in the past twenty-five years. From probes that detect particular molecules, to compounds that localise to specific organelles; this area of chemical biology is now host to an abundance of elegant molecular design.[1–4] When designing new fluorophores, minor changes in chemical structure can result in marked differences in cellular behaviour and localisation, and while many of these changes can be attributed to fairly rational design choices, it is often the case that unexpected behaviours arise.[5] It is, therefore, important to consider these results with respect not only to the intended application but also to the physical and molecular properties of the compound. Physicochemical descriptors such as logP, pK_a, polar surface area and membrane permeability will all affect cellular localisation since each cellular compartment exhibits varying environmental properties (Fig. 1A), and having a firm understanding of how the modulation of these physicochemical parameters influences the observed behaviour will assist in the design of more selective compounds.[6–9]

The incorporation of cellular recognition motifs also adds complexity when analysing new fluorophores and poses a number of questions.[10] For example, does the targeting motif exhibit passive behaviour e.g. utilising an intrinsic intracellular electrochemical gradient? Or is it "active" i.e. requiring metabolism, or recognition by a fixed concentration of a cellular species? It is important to bear these questions in mind when designing imaging experiments since variables such as fluorophore concentration, treatment time, culture conditions and cell type will all impact the observed imaging results and level of perturbation to the biological process under observation.

To understand cellular localisation, an imaging approach is most often employed.[11] Automated computational methods for analysing fluorescence images are also extremely beneficial for

a. LightOx Limited, 65 Westgate Road, Newcastle upon Tyne, NE1 1SG, UK
b. Department of Biosciences, Durham University, South Road, Durham, DH1 3LE, UK
c. Department of Physics & Astronomy, University College London, Gower Street, London, WC1E 6BT, UK
d. Department of Chemistry, Durham University, Science Laboratories, South Road, Durham, DH1 3LE, UK
e. High Force Research Limited, Bowburn North Industrial Estate, Bowburn, Durham, DH6 5PF, UK
f. Centre for Advanced Instrumentation, Department of Physics, Durham University, South Road, Durham, DH1 3LE, UK
† Joint first authors
* Corresponding authors
Electronic Supplementary Information (ESI) available: [details of any supplementary information available should be included here]. See DOI: 10.1039/x0xx00000x

high-throughput work, for example in proteomics[12] or for analysis of combinatorial libraries of fluorescent compounds.[13] Predictive models for subcellular localisation are becoming increasingly beneficial for the design of new fluorophores, [14] and there is a great need for informative accounts of subcellular behaviour; the more structure-based imaging case-studies there are, the better informed we can be in making molecular design choices.[15]

We recently reported a new class of diphenylacetylene that elicits cytotoxic activity when activated by UV, violet and corresponding two-photon near-IR irradiation.[16,17] When designing new chemical derivatives of this structural class, small modifications in chemical structure often resulted in distinct localisation behaviour and it became apparent that a more holistic approach to the understanding of these changes was necessary in order to inform more effective design choices. Therefore, an investigation into the effect of changing molecular structure upon subcellular localisation within a family of related diphenylacetylenes (Fig. 1) was conducted.
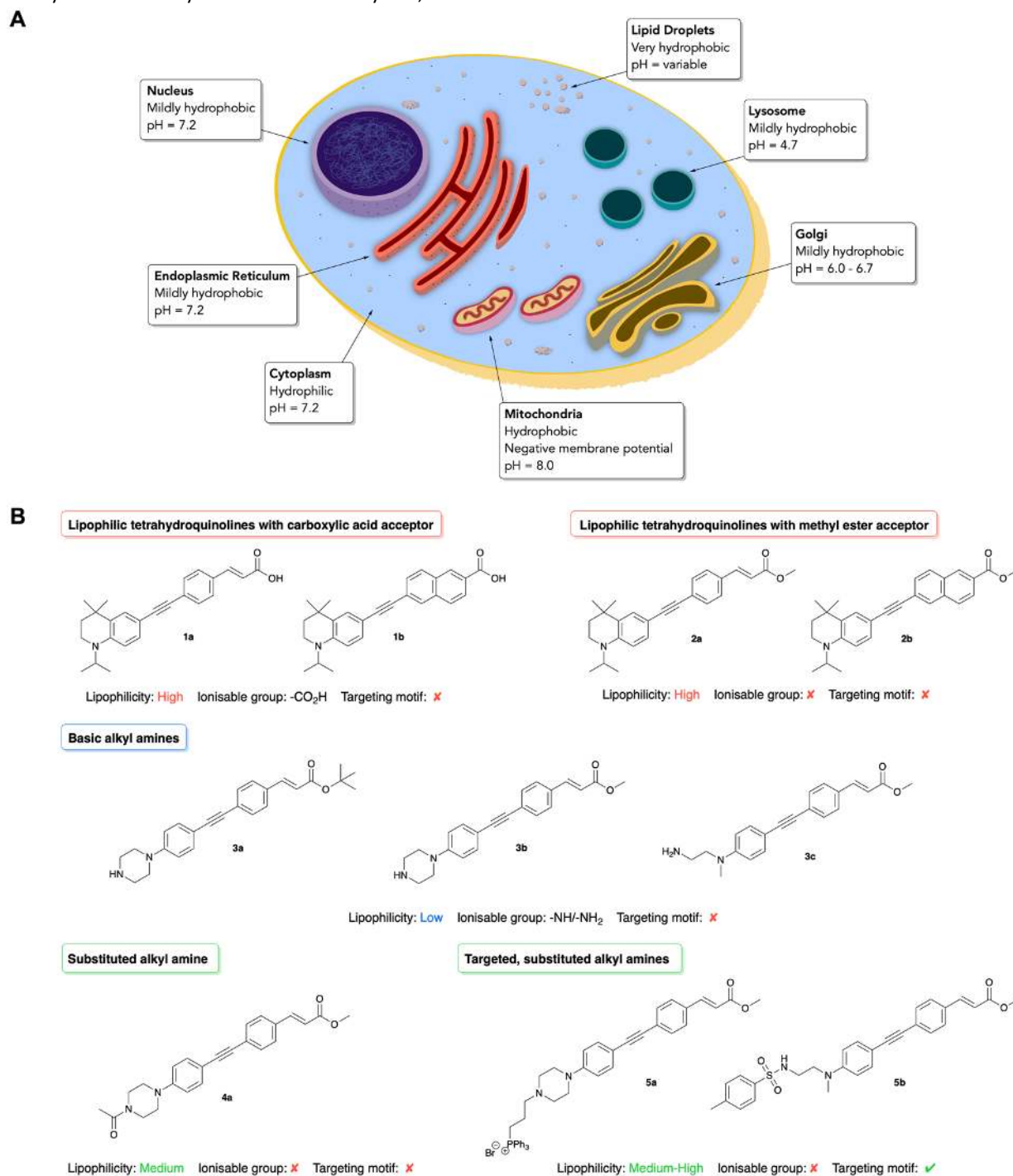

Fig. 1 A) General characteristics of cellular compartments in human cells.[18] B) Series of fluorescent diphenylacetylenes with differing substituents, targeting moieties and physicochemical properties

Organic & Biomolecular Chemistry

ARTICLE

Results and Discussion

Synthesis

Lipophilic acids **1a** and **1b** (syntheses reported previously[16,19]) and esters **2a** and **2b** were synthesised by the Sonogashira coupling of 6-iodo-tetrahydroquinoline **6** (synthesis reported previously[20]) with acetylenes **7a**[16] and **7b**[19] (Scheme 1).
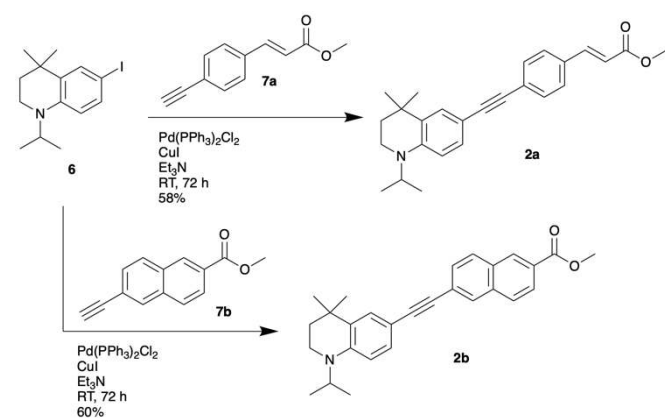

Scheme 1 Synthesis of lipophilic esters **2a** and **2b**.

The tetrahydroquinoline moiety employed in these compounds is an excellent π-donor for a donor-acceptor fluorophore due to its rigid structure, but the *gem*-dimethyl and *iso*propyl groups also provide a significant degree of lipophilicity. We anticipated that it would be difficult to direct such hydrophobic compounds towards more polar cellular environments and, hence, we designed an alternative, less lipophilic, phenylpiperazine-based π-donor scaffold. Phenylpiperazines are widely used in therapeutics due to their often-favourable effects on pharmacokinetic properties, but we also envisaged the free secondary amine would be a useful attachment point for moieties known to direct cellular localisation.
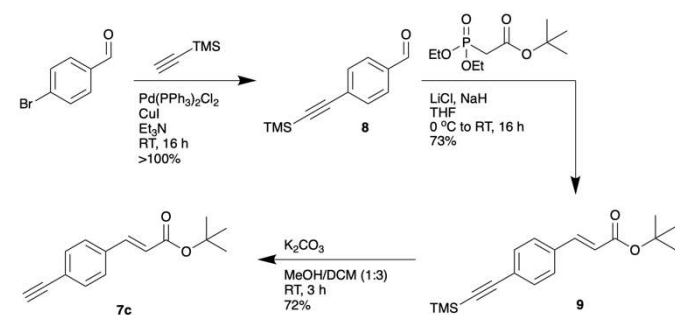

Scheme 2 Synthesis of *tert*-butyl alkyne acceptor moiety **8a**.

Phenylpiperazine diphenyl acetylenes **3a** and **3b** were synthesised according to Scheme 3, in which commercially available 1-phenylpiperazine was iodinated using ICl in AcOH/H$_2$O in a 63% yield on a multi-gram scale. Sonogashira coupling with alkynes **7a**[16] and **7c** (Scheme 2) was conducted with 5 mol% Pd(PPh$_3$)$_2$Cl$_2$/CuI in triethylamine. Iodo-phenylpiperazine **10** is poorly soluble in triethylamine at RT, hence, the solution was heated to 60 °C in order to achieve an acceptable conversion of the starting iodide. SiO$_2$ chromatography, followed by recrystallisation from MeOH or MeCN provided the desired **3a** and **3b** in acceptable to good yields.
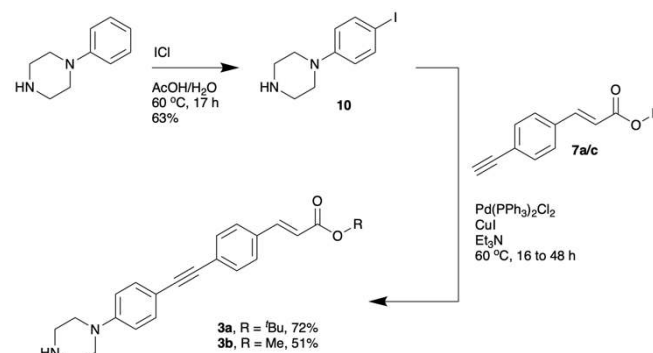

Scheme 3 Iodination of 1-phenylpiperazine to provide key π-donor building block **10**, followed by Sonogashira coupling to give corresponding diphenylacetylenes **3a** and **3b**.

We also anticipated that the corresponding primary amine **3c** would be significantly more polar than the tetrahydroquinoline-based compounds and, accordingly, devised an analogous synthetic route (Scheme 4) employing a Sonogashira coupling of iodoaniline derivative **14**. Acylation of 4-iodo-*N*-methylaniline with chloroacetyl chloride, followed by insertion of the primary amine group using Gabriel chemistry provided 2-amino-*N*-phenylacetamide **13**. Reduction using BH$_3$.Me$_2$S yielded the target aniline **14** which was coupled to **7a** to provide primary amine diphenylacetylene **3c** in a 58% yield.
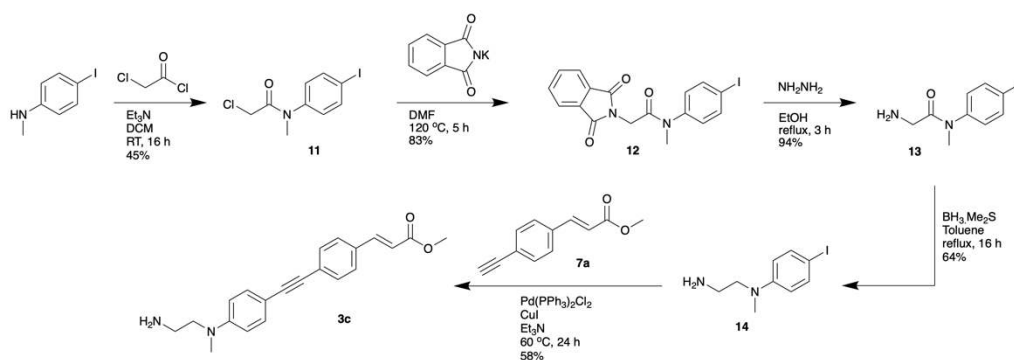
Scheme 4 Synthesis of amine-substituted diphenylacetylene **3c.**

The reactive amine groups of **3a**-**3c** enable further modulation of the properties of the compounds through a single step conversion, i.e. acylation, alkylation or sulfonylation. To this end, we exemplified acylation *via* reaction of **3b** with acetyl chloride to provide the *N*-Ac diphenylacetylene **4a** in an excellent yield (Scheme 5). Alkylation with commercially available (3-bromopropyl)triphenylphosphonium bromide was achieved by heating a solution of **3b** in DMF with K_2CO_3 to provide triphenylphosphonium-linked **5a** in a 66% yield. Triphenyphosphonium cations are widely used to encourage accumulation in the mitochondrial matrix due to the significant negative mitochondrial membrane potential.[21,22] We also sulfonylated **3c** using tosyl chloride (Equation 1) to provide the *N*-tosyl-piperazine diphenylacetylene, **5b**; tosyl sulphonamide groups have been employed as ER targeting moieties in a variety of fluorophores.[23,24]
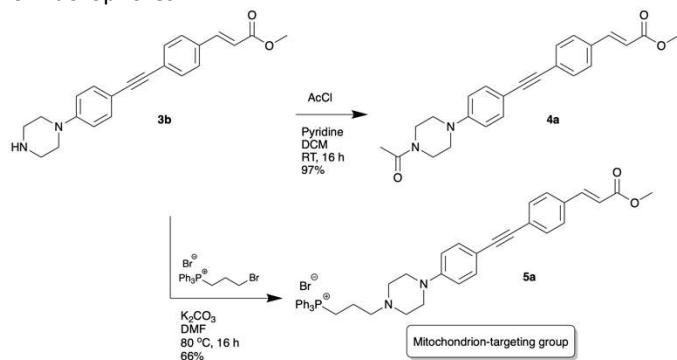
Scheme 5 Acetylation of **3b** to give *N*-Ac diphenylacetylene **4a** and addition of a mitochondrial targeting group **5a**.
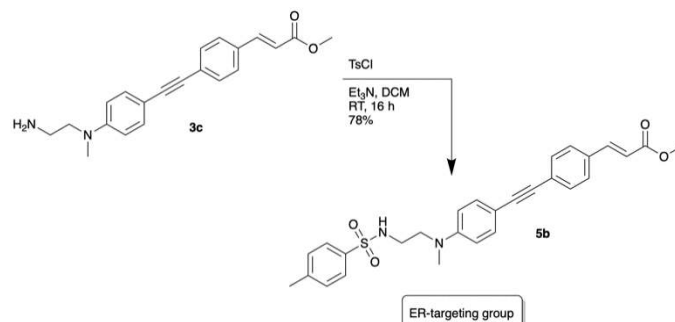
Equation 1 Sulfonylation of **3c** to provide an ER-targeting compound **5b**.

Photophysical characterisation

All of the compounds exhibited photophysical properties (Table 1) that were characteristic of other donor-acceptor diphenylacetylenes.[16,17,19] The compounds exhibited absorption (Fig. 2, Table 1 and ESI Section 2) bands at around 300 nm ($S_0 \rightarrow S_2$) and 360-400 nm ($S_0 \rightarrow S_1$) due to the formation of intramolecular charge transfer excited states as a result of the presence of strong π-donor/acceptor moieties (Figure 2A). Generally, those compounds with a THQ donor moiety (**1a**-**2b**) exhibited absorptions at longer wavelength and with larger extinction coefficients compared to those with the more electron deficient donor structures (**3a-5d**). Excitation led to highly solvatochromatic fluorescence emission (Figure 2B) in all compounds, with a large bathochromic shift evident in EtOH, indicating that polar solvents stabilise the emissive S_1 state. In toluene, the compounds exhibited quantum yields of up to 0.89 and mean lifetimes of around 1.5 ns, but a significant reduction in both was observed in EtOH, perhaps due to aggregation in this much more polar environment. The alkyl amines, **3a-3c**, also exhibited a significantly reduced quantum yield in toluene, possibly also due to aggregation effects of these more polar compounds. All compounds exhibited multiexponential fluorescence decay dynamics in both solvents, indicating the presence of multiple emissive conformations or environments, each with a distinct lifetime (see ESI, Table 1).[16]
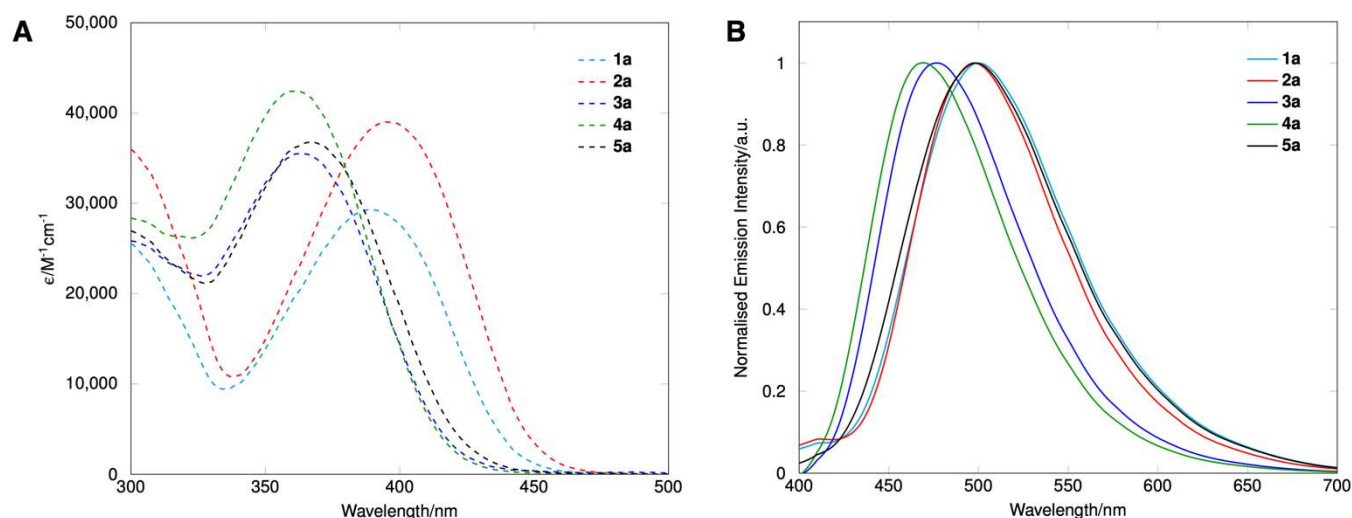
Figure 2 (A) Absorption spectra of compounds **1a**, **2a**, **3a**, **4a** and **5a** in toluene (100 μM). (B) Normalised emission spectra of compounds **1a**, **2a**, **3a**, **4a** and **5a** in toluene (10 μM).

Table 1: Photophysical properties of compounds **1a**-**5b** in toluene and EtOH.

Compound	Solvent	λ_{abs}(max)/nm	ε/M^{-1}cm^{-1}	λ_{em}(max)/nm	ϕ	$<\tau>$/ns
1a	Toluene	390	29287	500	0.67	1.62
	EtOH	387	25120	525	0.13	0.20
1b	Toluene	392	43273	466	0.84	1.62
	EtOH	387	24125	548	0.13	0.15
2a	Toluene	395	39014	498	0.80	1.68
	EtOH	394	31017	555	0.06	0.11
2b	Toluene	392	56722	466	0.78	1.67
	EtOH	387	30825	553	0.15	0.13
3a	Toluene	362	35500	477	0.19	1.58
	EtOH	357	37885	521	0.12	0.08
3b	Toluene	362	23873	482	0.23	1.61
	EtOH	352	15713	503	0.14	0.11
3c	Toluene	377	25681	479	0.21	1.45
	EtOH	367	32355	527	0.06	0.12
4a	Toluene	361	42421	468	0.97	1.45
	EtOH	357	27933	535	0.10	0.06
5a	Toluene	367	36816	498	0.72	1.64
	EtOH	358	29209	503	0.13	0.09
5b	Toluene	382	34973	478	0.89	1.58
	EtOH	377	31767	535	0.13	0.10

Imaging & cellular characterisation

We next conducted a series of imaging experiments to characterise and understand the cellular localisation of the compounds and attempted to relate their respective behaviours to the differences in molecular structure. HaCaT keratinocytes were treated with varying concentrations of each compound and incubated for 1 hour, whereupon they were imaged using a Zeiss 880 confocal microscope.

Whole cell fluorescence emission scan (lambda scan) experiments with each compound were carried out in order to understand the differences in *in cellulo* fluorescence emission behaviour. The lambda scans (see ESI Section 3) were

conducted on groups of whole cells, and to minimise photobleaching and the effect of z-drift whilst imaging, a large pinhole size of 5 Airy Units was used to allow low laser power, maximal depth coverage and fast scan speeds.

Each compound displayed the broad emission that is characteristic of donor-acceptor diphenylacetylenes due to emission taking place from excited states that exhibit a variety of angles about the freely rotatable central acetylene,[16,25] and also showed a similar λ_{max} to those obtained in toluene. The most obvious differences between compounds are shown in Fig. 3; foremost of which is the blue-shift in the emission of the acids **1a/1b** compared to the corresponding esters **2a/2b**. This is likely due to deprotonation of the carboxylic acid of **1a/1b** that causes a reduction in the dipolar nature of the excited

state. Local polarity also appears to play a role; the basic amine compounds **3a**-**c** showed more red-shifted emission spectra, in line with the prediction that their amine groups - protonated at physiological pH - cause a shift in localisation to a more polar environment compared to the tetrahydroquinoline-based compounds. A further red shift was observed in cells treated with **4a**, indicating that this compound localises to even more hydrophilic compartments (*vide infra*). Targeted derivatives, **5a/5b,** showed similar lambda scans to their parent compounds (see ESI Section 3).
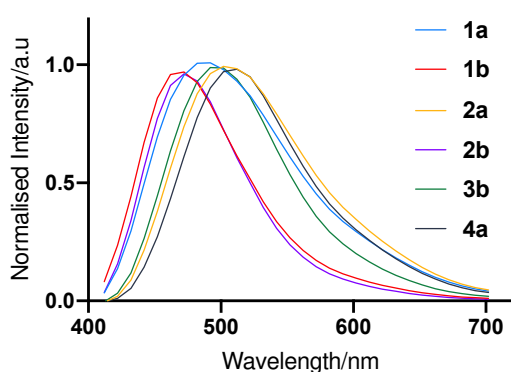

Figure 3 Whole cell fluorescence emission scans of HaCaT keratinocytes treated with **1a**, **1b**, **2a**, **2b**, **3b** and **4a** (1 µM). Emission was recorded on a confocal microscope via a lambda scan with laser excitation of 405 nm.

With the emission behaviour on a whole cell basis understood, we next sought to conduct a series of imaging experiments to gain insights into the differences in localisation behaviour as a function of compound structure. A co-localisation approach (see ESI Section 4) was employed in which HaCaT keratinocytes treated with **1a**-**5b** were co-treated with a range of commercially available organelle-specific dyes with different absorption/emission properties. By spectral analysis, it is possible to extract the components of the overall fluorescence signal from each compound and hence overlay the two to understand the extent of overlap of the signals. For the analysis, we used a combination of visual inspection along with a Pearson's Correlation Coefficient (PCC) statistical analysis (see ESI Section 6). PCC measures the covariance of each pixel, and ranges from +1 to -1, indicating a perfect linear relationship and a perfect inverse relationship, respectively.[15]

Localisation to the endoplasmic reticulum was first assessed using BODIPY ER-Tracker™ Red (BODIPY TR Glibenclamide)[26] which can be excited at 587 nm and emits with a peak emission wavelength at 615 nm. As shown in Fig. 4, both of the acids, **1a** and **1b**, exhibit significant co-localisation with the ER-Tracker (PCC = 0.71 and 0.80, respectively) along with general lipophilic staining. Both compounds also appeared to localise to the nuclear envelope, highlighted by arrows in Fig. 4, as is typical for compounds that interact with the ER due to the continuity between the structures.[27] We also used Nile Red as a general lipophilic stain,[28] which similarly showed significant co-localisation with **1a** and **1b** (PCC = 0.80 and 0.81, respectively) and, hence, we can characterise these compounds as non-specific lipophilic and ER dyes (see ESI Section 4 & 7).
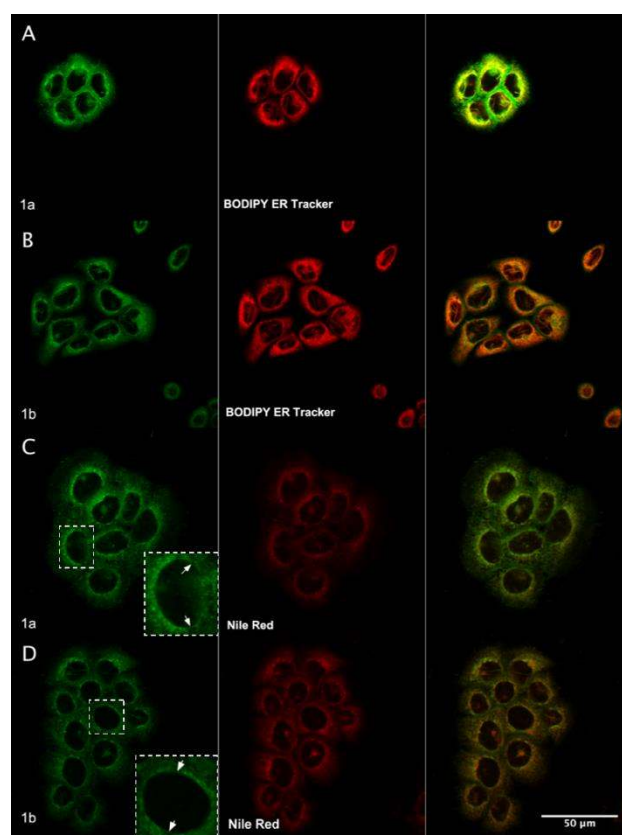

Figure 4 Co-localisation images of lipophilic acids **1a** and **1b** compared to BODIPY ER-Tracker™ Red and Nile Red.

ARTICLE

In contrast to the diffuse, non-specific localisation exhibited by lipophilic acids **1a** and **1b**, the behaviour of the corresponding methyl esters **2a** and **2b** was characterised by the presence of bright punctate spots distributed throughout the cells (Figure 5).[17] These spots were shown to colocalise with a BODIPY™ 493/503 Lipid Droplet probe (PCC = 0.65 and 0.66), and given the high degree of lipophilicity of **2a** and **2b** (simulated logP = 5.95 and 6.89, respectively) it is reasonable to suggest that the compounds are trafficked to lipid rich areas, and are perhaps actively packaged into vesicles for transport out of the cell. The subtle nuclear envelope staining evidenced in the case of **1a** and **1b** was not evident with the corresponding esters, but some mitochondrial staining according to MitoTracker™ Deep Red FM co-localisation was evident, although a low PCC value (PCC = 0.33 and 0.32, respectively) indicated that this was not a very specific effect, with the majority of the fluorescence signal evident in the bright punctate structures.
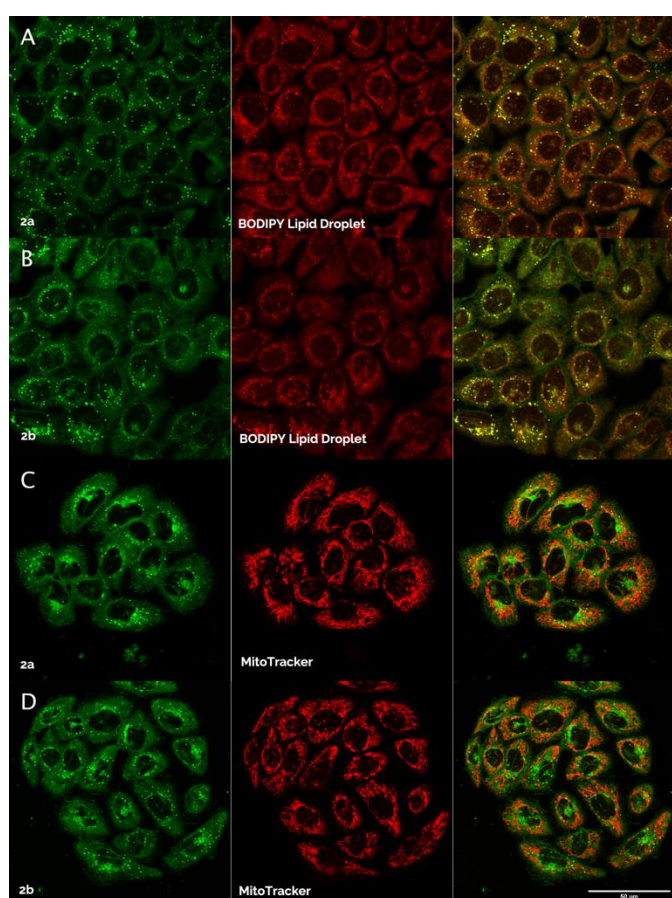

Figure 5 Co-localisation images of lipophilic esters **2a** and **2b** compared to Nile Red and MitoTracker Red™.

Upon moving from the highly lipophilic tetrahydroquinoline diphenylacetylenes **1a**-**2b** to the more polar **3a**-**3c**, a significant shift in the localisation behaviour was observed. The presence of the strongly basic unfunctionalised amine groups in **3a**-**3c** would suggest that these compounds localise to cellular compartments in which the pH was lower.[29] Indeed, **3a**-**3c** were shown to exhibit distinct lysosomal localisation according to

significant co-localisation (PCC = 0.69, 0.63 and 0.73, respectively) with the lysosomal fluorophore, LysoTracker™ Deep Red (Fig. 6) although some subtle differences were evident between the three compounds. Comparing **3a** (*tert*-butyl ester) with **3b** (methyl ester), it was apparent that **3a** showed some evidence of localisation in the endoplasmic reticulum (PCC compared to ER-Tracker = 0.48), especially as much of the fluorescence signal was polarised towards one side of the nucleus in some cells. **3a** also exhibited some overlap with the lipophilic fluorophore (PCC = 0.42), Nile Red, suggesting that the presence of the hydrophobic *tert*-butyl ester group causes enough of an increase in logP (estimated[30] logP = 4.49 for **3a** versus 3.41 for **3b**) to bring about some non-specific hydrophobic interactions with more lipophilic cellular compartments (see ESI). The less hydrophobic compounds, **3b** and **3c** showed more specific lysosomal localisation according to the statistical analysis (see ESI), although with some subtle indicators of Golgi, ER and mitochondrial staining.
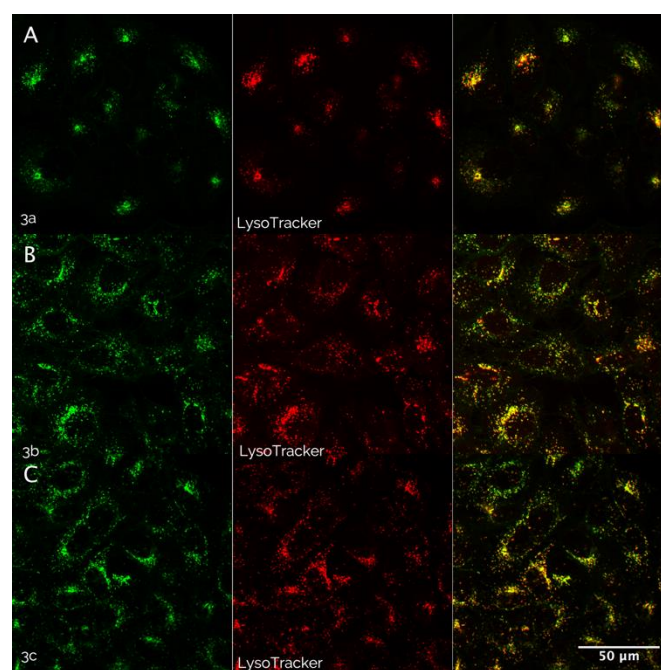

Figure 6 Co-localisation images of basic alkyl amines **3a-c** compared to LysoTracker™ Deep Red.

When the localisation behaviour of **3b** was compared to the corresponding *N*-acetyl phenylpiperazine **4a**, a striking difference was observed. Once the basic phenylpiperazine free amine is blocked, **4a** is likely to remain neutrally charged in cells since the pK_aH of the conjugated amine group is unlikely to be high enough to be protonated at physiological pH due to significant π-donation into the extended diphenylacetylene structure. **4a** exhibited much more membrane-based localisation, where it was brightest towards the exterior of the cell and around the nuclear envelope (Fig. 7). The compound exhibited very weak correlation with the ER and mitochondria (PCC = 0.27 and 0.09, respectively), in contrast with **3a**-**3c**, although some lysosomal co-localisation was evident (PCC = 0.22), perhaps suggesting that **4a** is a substrate for enzymatic

degradation through deacetylation, releasing the secondary amine **3b**. The cellular behaviour of **4a** was distinct from all the compounds studied, and underlined the effect of the removal of ionisable groups along with a structure of relatively higher polarity (estimated[30] logP of **4a/2a** = 4.03/5.95) in guiding the compound to more polar cellular environments.

Where the other compounds had displayed somewhat heterogenous behaviour, triphenylphosphonium-substituted **5a** was found to exhibit much more specific localisation. As shown in Fig. 8, co-localisation studies involving the Mitotracker™ mitochondrial dye and **5a** highlighted a strong correlation (PCC = 0.71) between the two signals, indicating that the compound was likely to be localised in the mitochondria, as anticipated.[22] Statistical analysis also indicated strong correlation with the ER (PCC = 0.75) and lipophilic (PCC = 0.63) dyes, however, it was adjudged that the physiology of those structures associated with **5a** were distinct from that of the ER and lipid environments (particularly in comparison with **2a/2b** for the latter), and hence underlined the need to carefully examine the cellular images rather than rely solely on the statistical analysis.
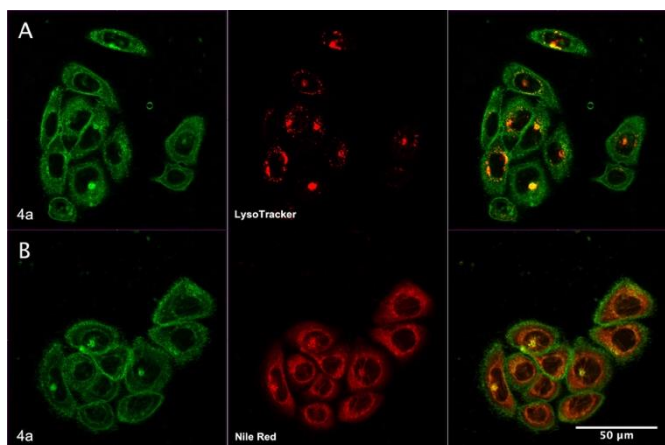

Figure 7 Colocalisation images of acyl amine **4a** compared to LysoTracker™ Deep Red and Nile Red.

Imaging of the tosyl sulphonamide substituted compound **5b** (Fig. 9) indicated co-localisation with the ER dye as initially anticipated (PCC = 0.62),[24,31–33] however, analysis of the images suggested that this was not an entirely specific effect. Indeed, while weaker correlations were evident with Mitotracker™ (PCC = 0.41) or Lysotracker™ (PCC = 0.46), the lipophilic dye Nile Red was shown to exhibit significant co-localisation with **5b** as indicated by a high PCC value (0.86). Given the relatively high lipophilicity of **5b** (simulated logP = 5.2), as a result of the presence of the tosyl group, this behaviour is not entirely unexpected. In fact, comparison with **1a** and **1b** shows that **5b** behaves similarly to the lipophilic carboxylate compounds i.e. general localisation in non-polar cellular environments such as the ER, although without the very bright punctate spots displayed by the even more lipophilic **2a/2b**. Indeed, the correlation statistics actually showed that lipophilic carboxylates **1a/1b** displayed more specific ER localisation than **5b** (see ESI) and are, therefore, more appropriate ER

fluorophores than the sulphonamide **5b** within this series of diphenylacetylene fluorophores. Perhaps by reducing the lipophilicity of derivatives of **5b** and/or increasing the linker length for the sulphonamide moiety, more specific ER localisation could be observed. The subtleties in the fluorescence localisation behaviour of **5b** does, however, underline the need to conduct co-localisation studies that employ several fluorophores and techniques along with careful analysis of each image.
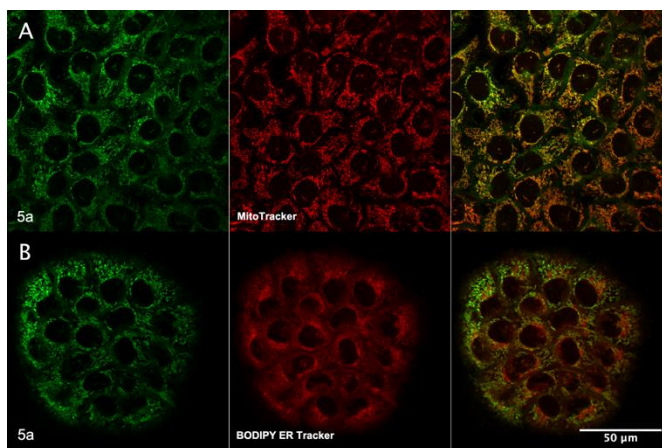
Figure 8 Co-localisation images of substituted triphenylphosphonium compound **5a** compared to MitoTracker™ Red and ER tracker Red.
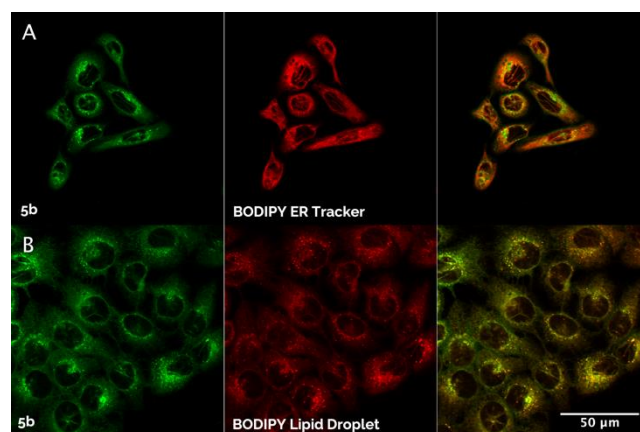
Figure 9 Colocalisation images of sulphonamide **5b** compared to ER tracker Deep Red and Nile Red.

Next, the relative intensities of the fluorescence in a cellular environment was assessed. Individual wells of cultured HaCaT epithelial cells were pre-treated with the same concentration of each compound (1 µM) and then imaged. Using ImageJ for the analysis, thresholding was applied to select the cells within the images and omit any background devoid of cells, and the average intensity per pixel in each image was then calculated and used as the comparison metric. The entirety of each cell was included in this analysis rather than just the labelled regions in order to ensure that, whether a compound localised in highly punctate spots or exhibited more broad, diffuse localisation, the variation was properly accounted for to give a valid comparison

between compounds, rather than just focusing on different organelles.

Figure 10 Normalised whole-cell relative fluorescence intensity of each compound (1 µM) in HaCaT keratinocytes. A 405 nm laser was used to excite the compounds.

In these experiments (Fig. 10 and ESI Section 5), it was clear that primary amine **3c** and the corresponding *N*-tosyl sulphonamide **5b** provided the most intense fluorescence signal under these experimental conditions. The greater intensity may be a functi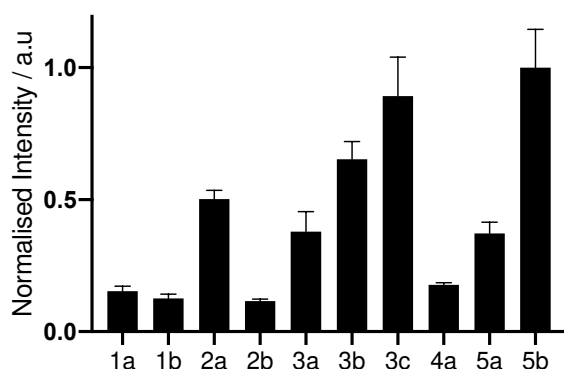on of the 405 nm excitation being closer to the λ_{max} of **3c** and **5b** (377 & 382 nm, respectively, in toluene) as a result of the stronger donor capability of the *N*,*N*-disubstituted aniline structure in comparison to the more strained phenylpiperazine systems. Conversely, however, those compounds with the even stronger donor, the rigid tetrahydroquinoline of **1a**-**2b**, exhibited relatively weaker fluorescence signal, suggesting that cellular localisation plays a greater role in the relative intensity within this family of compounds. Furthermore, the other free amines, particularly **3b**, exhibited similarly strong fluorescence to **3c**, and it may be that the lysosomal environment is particularly insulating for these compounds, limiting non-radiative processes that are presumably more prevalent in a more aqueous environment. This change in fluorescence intensity as a function of environment is further echoed when comparing the acid **1a** (ER and cytoplasmic localisation – more polar) to the corresponding methyl ester **2a** (lipid droplets – less polar), although those compounds with the naphthalene acceptor (**2a/2b**) appeared to be outliers from this trend. The substituted amine **4a** also showed weaker fluorescence intensity compared to the related **3b** and **5a**, which correlates to the observed, more polar, membrane-based localisation and presumably translates to an increase in non-radiative quenching of the excited state – a common occurrence with donor-acceptor fluorophores in more polar, aqueous enviroments.[34]

The major influence of the local environment on the observed fluorescence was further underlined when we examined the effect of pH. Solutions of each compound were prepared in buffers of pH 5, 7.5 and 9 in order to reflect the typical pH that the compounds may encounter in different cellular compartments, and the emission spectrum of each solution was recorded between 400-700 nm with a common, fixed excitation wavelength of 360 nm. The emission spectra at each pH were compared (see ESI, Section 6) and showed that the fluorescence behaviour of compounds possessing ionisable groups (**1a/1b**, **3a-c**, **5a/5b**) was heavily influenced by pH changes, while those compounds lacking ionisable groups (**2a/2b** and **4a**) exhibited only minor differences as a function of pH. The carboxylic acids, **1a/1b**, exhibited a blue-shift and a significant increase in intensity at pH 7.5 and 9 compared to the emission spectrum at pH 5, indicating that deprotonation of the carboxylic acid causes a major change in the excited state properties of these compounds. The basic amines, **3a**-**3c**, displayed a linear increase in emission intensity as the pH was increased from 5, to 7.5, to 9, along with a mild red shift (ca. 15 nm from pH 5 to 9 for **3a**), thus demonstrating that protonation of the basic amine group elicits an electron-withdrawing inductive influence upon the conjugated nitrogen atom that diminishes the strength of charge transfer and, hence, reduces fluorescence intensity. A very similar effect was also observed with **5a** due to the compound's basic tertiary amine group. The sulfonamide **5b** exhibited very similar emission spectra at pH 5 and 7.5, but a 20 nm blue-shift and minor increase in intensity was observed at pH 9, indicating that the emission behaviour of this compound is also modulated as the pH of the solution nears the pK_a of the sulfonamide proton.

The results of the whole-cell relative intensity experiments and the pH study demonstrate that, for fluorophores that are highly sensitive towards local environment, the observed fluorescence intensity within a cell is not simply a function of the quantum yield. This is foremost evidenced by compounds **3a-c**, which displayed the lowest quantum yields in the photophysical characterisation (Table 1) yet exhibited some of the highest intensities in the whole cell intensity study (Fig. 10) even whilst localising in an acidic environment that attenuates charge transfer from the key donor nitrogen atom in the conjugated diphenylacetylene structure according to the pH experiments. It is, therefore, clear that cellular compartments exhibit unique environmental and solvation characteristics whose effects on photophysical properties such as fluorescence intensity are difficult to predict *a priori* using measurements determined in a single-component system. This underlines the need to undertake careful comparative studies involving both cellular and solvent-based measurements to inform meaningful predictions of cellular fluorescence behaviour.

We also performed a series of photostability experiments comparing the bleaching rate of each compound in live and fixed (PFA) cells in order to assess their suitability as a general class of fluorophore for a range of imaging experiments. As shown in Fig. 11, the compounds typically exhibited similar $T_{1/2}$ in live and fixed cells although generally with a slight increase in fixed cells as is often typical. However, while the photophysical properties of the compounds broadly remained similar upon fixation, the cellular localisation was found to vary significantly (see ESI, Section 8).
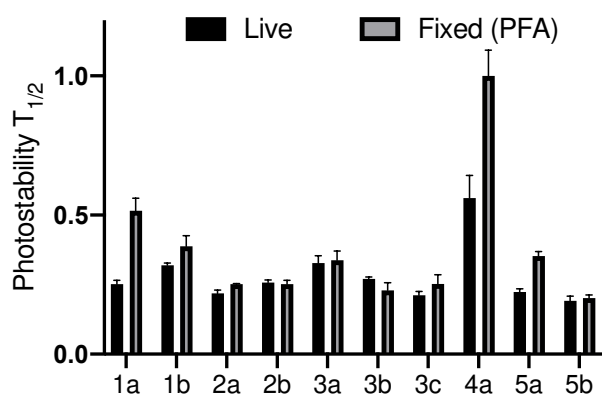
Figure 11 Photostability assessment of each compound in live and fixed HaCaT keratinocytes. A 405 nm laser was used to excite the compounds.

Compound	LogP	LogD^a	pK_a^{b}	pK_aH^c	Localisation
1a	5.13	2.17	4.5	-	ER Lipophilic areas
1b	6.79	3.83	4.5	-	ER Lipophilic areas
2a	5.95	5.95	-	-	Lipid droplets Lipophilic areas
2b	6.89	6.89	-	-	Lipid droplets Lipophilic areas
3a	4.49	3.27	-	8.6	Lysosome
3b	3.41	2.19	-	8.6	Lysosome
3c	3.45	2.50	-	8.3	Lysosome
4a	4.03	4.03	-	3.2	Cell membrane Cytoplasm
5a	8.10	5.74	-	6.2	Mitochondria
5b	5.20	5.20	10.1	-	ER Lipophilic areas

Table 2: Calculated physical properties of compounds **1a-5b** related to cellular behaviour. All physical properties were calculated using ACD/I-Lab 2.0.[30] ^{a} LogD at pH 7.4. ^{b} pK_a of the strongest acidic proton. ^{c} pK_aH of the strongest basic group.

Significant changes in fluorescent probe localisation are common when cells are fixed due to changes in subcellular structure, membrane integrity and permeability, local polarity, pH and chemical modification. Given that the photophysical properties of the compounds are very similar when fixed and live cells are compared, we can be confident that the compounds remain unmodified on fixation using a variety of methods (paraformaldehyde, alcohols) but instead are subject to changes in localisation due to the effect of fixation on the cell, and hence, we had to exercise great care when analysing fluorescence data from fixed cell samples. In contrast, compounds **1a-5b** were found to exhibit highly consistent localisation in all live experiments, and have good utility in this modality for a variety of imaging applications.

With all of these analyses in hand, we can begin to draw meaningful molecular conclusions (Table 2) on the cellular behaviour of the compounds. Perhaps the most significant determinant of cellular localisation within this family is the presence (or absence) of ionisable groups, which tend to override the inherent hydrophobicity of the core diphenylacetylene structure. For those compounds without ionisable groups, structures with high logP values exhibit localisation in more lipophilic cellular compartments. Reduction of lipophilicity, as is the case when comparing the tetrahydroquinoline **2a** and the *N*-Ac phenylpiperazine **4a**, causes a pronounced shift to more membrane-based/cytoplasmic environments. The addition of cellular recognition motifs (**5a/5b**) resulted in selective uptake to those areas, although the sulphonamide **5b** showed relatively heterogenous localisation behaviour compared to the triphenylphosphonium compound **5a**. Importantly, **5a/5b** showed markedly different behaviour from their respective parent compounds (**3b** and **3c**, respectively), indicating that this structural class of fluorophore is suitable for derivatisation with other recognition motifs, and a wide variety of modifications could be easily implemented to further influence cellular localisation behaviour.[10]

Conclusions

A group of structurally varied diphenylacetylene fluorophores have been described and characterised as novel imaging agents for a variety of cellular experiments. We have shown that through modification of their component structures in a considered manner the localisation behaviour of this class of compound can be directly influenced. This was most obviously evidenced by examining the effect of going from a highly lipophilic tetrahydroquinoline donor system (**2a**) to a much more polar phenylpiperazine (**3b**) and to the corresponding *N*-acetyl compound (**4a**), where we observe a shift in localisation from lipid-based to lysosomal to membrane-based that is commensurate with the changes in logP/logD and pK_aH between structures. The observations and guidelines observed herein can assist in directing the design and synthesis of not only the next generation of this class of fluorophore but also of other donor-acceptor fluorophore systems, which are a burgeoning class of compound both in the cellular imaging arena and a wide range of other applications including liquid crystals, plastics and sensor applications.

Experimental

General chemical information

Reagents were purchased from Sigma-Aldrich, Acros Organics, Alfa-Aesar and Fluorochem. Reagents were purified, if required, by recrystallisation or distillation/sublimation under vacuum.

Solvents were used as supplied from Fisher Scientific or Sigma Aldrich, and dried before use if required with appropriate drying agents. Thin-layer chromatography (TLC) was conducted using Merck Millipore silica gel 60G F254 25 glass plates and/or TLC-PET foils of aluminium oxide with fluorescent indicator 254 nm (40 × 80 mm) with visualisation by UV lamp or appropriate staining agents. Flash column chromatography was performed using SiO_2 from Sigma-Aldrich (230-400 mesh, 40-63 µM, 60 Å), and monitored using TLC. NMR spectra were recorded using Varian VNMRS-700, Varian VNMRS-600, Bruker Avance-400 or Varian Mercury-400 spectrometers operating at ambient probe temperature. NMR peaks are reported as singlet (s), doublet (d), triplet (t), quartet (q), broad (br), septet (sept), combinations thereof, or as a multiplet (m), with reference to the following deuterated solvent signals: $CDCl_3$ ([1]H = 7.26 ppm, [13]C = 77.0 ppm), $(CD_3)_2SO$ ([1]H = 2.50 ppm, [13]C = 39.5 ppm). ESMS was performed using a TQD (Waters Ltd., UK) mass spectrometer with an Acquity UPLC (Waters Ltd., UK), and accurate mass measurements were obtained using a QtoF Premier mass spectrometer with an Acquity UPLC (Waters Ltd., UK). ASAP measurements were performed using an LCT Premier XE mass spectrometer and an Acquity UPLC (Waters Ltd., UK). IR spectra were recorded using a Perkin Elmer FTIR spectrometer. Physicochemical values were estimated using ACD/I-Lab 2.0 online software (https://www.acdlabs.com/resources/ilab/).[30]

Methyl (2*E*)-3-(4-{2-[4,4-dimethyl-1-(propan-2-yl)-1,2,3,4-tetrahydroquinolin-6-yl]ethynyl}phenyl)prop-2-enoate, 2a

A solution of compound **6**[20] (1.72 g, 5.22 mmol) in Et_3N (34 mL) was degassed by sonication, before the atmosphere was replaced with Ar. Compound **7a**[16] (1.02 g, 5.48 mmol), $Pd(PPh_3)_2Cl_2$ (370 mg, 0.53 mmol) and CuI (99 mg, 0.52 mmol) were added under Ar and the resultant suspension was stirred at RT for 72 h. The suspension was diluted with heptane, passed through a short Celite/SiO_2 plug and the extracts were evaporated to give a crude solid. This was purified by SiO_2 chromatography (9:1, heptane/EtOAc), followed by recrystallisation from EtOH to give compound **2a** as a yellow solid (1.16 g, 58%): ^{1}H NMR (700 MHz, $CDCl_3$) δ 1.22 (d, *J* = 6.6 Hz, 6H), 1.28 (s, 6H), 1.64 – 1.73 (m, 2H), 3.17 – 3.25 (m, 2H), 3.81 (s, 3H), 4.15 (hept, *J* = 6.6 Hz, 1H), 6.43 (d, *J* = 16.0 Hz, 1H), 6.64 (d, *J* = 8.7 Hz, 1H), 7.24 (dd, *J* = 8.6, 2.1 Hz, 1H), 7.36 (d, *J* = 2.1 Hz, 1H), 7.45 – 7.50 (m, 4H), 7.67 (d, *J* = 16.0 Hz, 1H); ^{13}C NMR (176 MHz, $CDCl_3$) δ 18.9, 29.9, 32.0, 36.5, 36.6, 47.2, 51.7, 86.8, 94.1, 108.0, 110.4, 117.6, 126.6, 127.9, 129.3, 130.8, 131.5, 131.5, 133.0, 144.2, 144.6, 167.4; IR (ATR) v_{max}/cm^{-1} 3031w, 2969m, 2930m, 2867w, 2190m, 1716s, 1632m, 1592s, 1433s, 1322s, 1269s, 1203s, 1168s, 1139s, 829m; MS(ES): *m/z* = 388.2 [M+H]$^+$; HRMS (ES) calcd. for $C_{26}H_{30}NO_2$ [M+H]$^+$: 388.2271, found 388.2271.

Methyl 6-{2-[4,4-dimethyl-1-(propan-2-yl)-1,2,3,4-tetrahydroquinolin-6-yl]ethynyl}naphthalene-2-carboxylate, 2b

A solution of compound **6**[20] (2.55 g, 7.75 mmol) in Et_3N (60 mL) was degassed by sonication, before the atmosphere was replaced with Ar. Compound **7b**[19] (1.41 g, 7.14 mmol),

$Pd(PPh_3)_2Cl_2$ (470 mg, 0.67 mmol) and CuI (132 mg, 0.69 mmol) were added under Ar and the resultant suspension was stirred at RT for 72 h. The suspension was diluted with heptane/EtOAc (9:1), passed through a short Celite/SiO_2 plug and the extracts were evaporated to give a crude solid. This was purified by SiO_2 chromatography (9:1, heptane/EtOAc), followed by recrystallisation from EtOH to give compound **2b** as a yellow solid (1.76 g, 60%): ^{1}H NMR (700 MHz, $CDCl_3$) δ 1.23 (d, *J* = 6.6 Hz, 6H), 1.30 (s, 6H), 1.66 – 1.73 (m, 2H), 3.18 – 3.27 (m, 2H), 3.98 (s, 3H), 4.16 (hept, *J* = 6.6 Hz, 1H), 6.66 (d, *J* = 8.6 Hz, 1H), 7.28 (dd, *J* = 8.6, 2.1 Hz, 1H), 7.41 (d, *J* = 2.1 Hz, 1H), 7.62 (dd, *J* = 8.5, 1.7 Hz, 1H), 7.82 (d, *J* = 8.6 Hz, 1H), 7.88 (d, *J* = 8.5 Hz, 1H), 8.01 (d, *J* = 1.5 Hz, 1H), 8.05 (dd, *J* = 8.6, 1.7 Hz, 1H), 8.56 (s, 1H); ^{13}C NMR (176 MHz, $CDCl_3$) δ 18.9, 29.9, 32.0, 36.5, 36.6, 47.2, 52.2, 87.1, 93.6, 108.1, 110.4, 124.4, 125.8, 127.4, 127.7, 129.1, 129.4, 129.4, 130.0, 130.8, 130.9, 131.3, 131.5, 135.3, 144.6, 167.1; IR (ATR) v_{max}/cm^{-1} 2969m, 2929m, 2867w, 2191m, 1717s, 1625m, 1605s, 1594s, 1434s, 1280s, 1188s, 1179s, 1096m, 892m; MS(ES): *m/z* = 412.2 [M+H]$^+$; HRMS (ES) calcd. for $C_{28}H_{30}NO_2$ [M+H]$^+$: 412.2271, found 412.2273.

Tert-butyl (2*E*)-3-(4-ethynylphenyl)prop-2-enoate, 7c

Et_3N (250 mL) was degassed by sparging with Ar for 1 h. 4-Bromobenzaldehyde (18.5 g, 100.0 mmol), $Pd(PPh_3)_2Cl_2$ (1.4 g, 2.00 mmol), CuI (0.38 g, 2.00 mmol) and trimethylsilylacetylene (15.2 mL, 110.0 mmol) were then added under Ar and the resultant suspension was stirred at RT for 16 h. The suspension was diluted with heptane, passed through a short Celite/SiO_2 plug and the extracts were evaporated to give a crude dark solid (24 g). This was purified by Kugelrohr distillation (130-150 °C, 9.0 Torr) to give compound **8** as an off-white solid (21.5 g, >100%), which was carried to the next step without further purification. *Tert*-butyl diethylphosphonoacetate (14.4 mL, 61.5 mmol) and LiCl (2.54 g, 60.0 mmol) were added to anhydrous THF (100 mL) at 0 °C and the resultant solution was stirred for 15 min, whereupon compound **8** (10.1 g, 50.0 mmol) was added. To this solution was slowly added DBU (8.2 mL, 55.0 mmol), and the resultant slurry was stirred at RT for 16 h. This was poured into crushed ice, and extracted with EtOAc. The organics were washed with H_2O and brine, dried ($MgSO_4$) and evaporated to give a crude white solid (18 g). This was purified by recrystallisation from heptane to give compound **9** as a colourless crystalline solid (10.99 g, 73%): ^{1}H NMR (400 MHz, $CDCl_3$) δ 0.25 (s, 9H), 1.53 (s, 9H), 6.36 (d, *J* = 16.0 Hz, 1H), 7.40 – 7.49 (m, 4H), 7.54 (d, *J* = 16.0 Hz, 1H). Compound **9** (10.95 g, 36.4 mmol) and K_2CO_3 (7.55 g, 54.6 mmol) were added to MeOH/DCM (200 mL, 1:3) and the resultant solution was stirred at RT for 3 h. The solution was diluted with DCM, and the organics washed with sat. NH_4Cl and H_2O, dried ($MgSO_4$) and evaporated to give a crude solid (8 g). This purified by recrystallisation from heptane to give compound **7c** as a colourless crystalline solid (5.96 g, 72%): ^{1}H NMR (600 MHz, $CDCl_3$) δ 1.53 (s, 9H), 3.17 (s, 1H), 6.36 (d, *J* = 16.0 Hz, 1H), 7.43 – 7.49 (m, 4H), 7.54 (d, *J* = 16.0 Hz, 1H); ^{13}C NMR (151 MHz, $CDCl_3$) δ 28.1, 79.0, 80.6, 83.2, 121.2, 123.5, 127.7, 132.5, 135.0, 142.4, 166.0; IR (ATR) v_{max}/cm^{-1} 3281m, 3064w, 3000w, 2980w,

2936w, 1691s, 1641m, 1370m, 1296s, 1153s, 1002m, 980m, 832s; MS(ASAP): m/z = 228.1 [M+H]$^+$; HRMS (ASAP) calcd. for C$_{15}$H$_{16}$O$_2$ [M+H]$^+$: 228.1150, found 228.1161.[35]

1-(4-Iodophenyl)piperazine, 10

To a vigorously stirred solution of 1-phenylpiperazine (20.5 mL, 134.0 mmol) in AcOH/H$_2$O (3:1, 84 mL) at 55 ^{o}C was added dropwise a solution of ICl (24.0 g, 148.0 mmol) in AcOH/H$_2$O (3:1, 124 mL). The resultant slurry was further stirred for 1 h and then cooled to RT and stirred for a further 16 h. The slurry was poured into crushed ice, and 20% aq. NaOH added until the solution was at pH 13. The resultant precipitate was isolated by filtration, washed with H$_2$O and dried to give a crude yellow solid. This was purified by recrystallisation from MeOH/H$_2$O (1:1) to give compound **10** as a beige solid (24.2 g, 63%): ^{1}H NMR (600 MHz, CDCl$_3$) δ 2.97 – 3.03 (m, 4H), 3.07 – 3.14 (m, 4H), 6.65 – 6.69 (m, 2H), 7.48 – 7.52 (m, 2H); ^{13}C NMR (151 MHz, CDCl$_3$) δ 45.9, 49.9, 81.4, 118.0, 137.7, 151.3; IR (ATR) v_{max}/cm^{-1} 3032w, 2955w, 2829m, 1582m, 1489m, 1243s, 914m, 803s; MS(ASAP): m/z = 289.0 [M+H]$^+$; HRMS (ASAP) calcd. for C$_{10}$H$_{13}$N$_2$I [M]$^+$: 288.0124, found 288.0114.[36]

Tert-butyl (2*E*)-3-(4-{2-[4-(piperazin-1-yl)phenyl]ethynyl}phenyl)prop-2-enoate, 3a

Et$_3$N (80 mL) was degassed by sparging with Ar for 1 h. Compound **10** (2.16 g, 7.5 mmol), compound **7c** (1.80 g, 7.88 mmol), Pd(PPh$_3$)$_2$Cl$_2$ (260 mg, 0.39 mmol) and CuI (71 mg, 0.39 mmol) were then added under Ar and the resultant suspension was stirred at 60 ^{o}C for 24 h. The solvent was then evaporated to give a crude solid which was purified by SiO$_2$ chromatography (9:1, DCM/MeOH, 1% Et$_3$N) and then recrystallisation from MeOH to give compound **3a** as a yellow solid (2.11 g, 72%): ^{1}H NMR (400 MHz, CDCl$_3$) δ 1.53 (s, 9H), 3.22-3.28 (m, 4H), 3.38-3.45 (m, 4H), 6.37 (d, J = 15.9 Hz, 1H), 6.77 – 6.95 (m, 2H), 7.33 – 7.53 (m, 6H), 7.56 (d, J = 15.9 Hz, 1H); ^{13}C NMR (176 MHz, CDCl$_3$) δ 28.2, 80.6, 87.8, 92.2, 113.1, 115.2, 120.5, 125.5, 127.8, 127.8, 131.7, 132.8, 133.9, 142.7, 166.2; IR (ATR) v_{max}/cm^{-1} 2967w, 2916w, 2830w, 2212w, 1687s, 1629m, 1595m, 1518m, 1326m, 1241m, 1159m, 1128m, 986m, 831s, 819s; MS(ASAP): m/z = 389.2 [M+H]$^+$; HRMS (ASAP) calcd. for C$_{25}$H$_{29}$N$_2$O$_2$ [M+H]$^+$: 389.2229, found 389.2231.

Methyl (2*E*)-3-(4-{2-[4-(piperazin-1-yl)phenyl]ethynyl}phenyl)prop-2-enoate, 3b

Et$_3$N (150 mL) was degassed by sparging with Ar for 1 h. Compound **10** (4.50 g, 15.6 mmol), compound **7a** (3.05 g, 16.4 mmol), Pd(PPh$_3$)$_2$Cl$_2$ (550 mg, 0.78 mmol) and CuI (150 mg, 0.78 mmol) were then added under Ar and the resultant suspension was stirred at 60 ^{o}C for 24 h. The solvent was then evaporated to give a crude solid which was purified by SiO$_2$ chromatography (9:1, DCM/MeOH, 1% Et$_3$N) and then recrystallisation from MeOH to give compound **3b** as a yellow solid (2.74 g, 51%): ^{1}H NMR (600 MHz, DMSO-d_6) δ 2.82-2.94 (m, 4H), 3.14-3.24 (m, 4H), 3.73 (s, 3H), 6.67 (d, J = 16.0 Hz, 1H), 6.94 (d, J = 8.4 Hz, 2H), 7.39 (d, J = 8.4 Hz, 2H), 7.52 (d, J = 8.0 Hz, 2H), 7.67 (d, J = 16.0 Hz, 1H), 7.74 (d, J = 8.0 Hz, 2H); ^{13}C NMR (151 MHz, DMSO-d_6) δ 44.9, 47.5, 51.5, 87.6, 92.7, 110.7, 114.5, 118.3, 124.9,

128.6, 131.3, 132.5, 133.5, 143.6, 151.2, 166.6; IR (ATR) v_{max}/cm^{-1} 3039w, 2952w, 2909w, 2830w, 2204w, 2173w, 1698s, 1630s, 1593m, 1518m, 1312m, 1243s, 1168s, 987m, 831s, 817s; MS(ASAP): m/z = 347.2 [M+H]$^+$; HRMS (ASAP) calcd. for C$_{22}$H$_{23}$N$_2$O$_2$ [M+H]$^+$: 347.1760, found 347.1736.

2-Chloro-*N*-(4-iodophenyl)-*N*-methylacetamide, 11

4-Iodo-*N*-methylaniline (13.9 g, 59.7 mmol) was dissolved in DCM (100 mL), whereupon chloroacetyl chloride (5.2 mL, 65.7 mmol) and Et$_3$N (9.2 mL, 65.7 mmol) were added and the resultant mixture was stirred for 16 h at RT. The solution was then diluted with DCM, washed with sat. NH$_4$Cl and H$_2$O, dried (MgSO$_4$) and evaporated to give a crude solid. This was purified by SiO$_2$ chromatography (8:2, heptane/EtOAc) to give compound **11** as an off-white solid (8.26 g, 45%): ^{1}H NMR (600 MHz, CDCl$_3$) δ 3.28 (s, 3H), 3.83 (s, 2H), 6.95 – 7.06 (m, 2H), 7.78 (d, J = 8.1 Hz, 2H); ^{13}C NMR (151 MHz, CDCl$_3$) δ 37.9, 41.2, 93.9, 129.0, 139.3, 142.4, 166.1; IR (ATR) v_{max}/cm^{-1} 2996w, 2947w, 1664s, 1480m, 1371m, 1260m, 1009m, 824m, 552s; MS (ASAP) m/z = 310.0 [M+H]$^+$; HRMS (ASAP) calcd. for C$_9$H$_{10}$ONICl [M+H]$^+$: 309.9496, found 309.9494.

2-Amino-*N*-(4-iodophenyl)-*N*-methylacetamide, 13

Compound **11** (8.23 g, 26.6 mmol) and potassium phthalimide (7.39 g, 39.9 mmol) were dissolved in DMF (40 mL) and the resultant mixture was heated to 120 ^{o}C and stirred for 5 h. The solution was cooled, and diluted with H$_2$O. The resultant precipitate was isolated by filtration, washed with H$_2$O and then recrystallised from EtOH to give compound **12** as a white solid (9.26 g, 83%), which was carried directly to the next step. Compound **12** (9.2 g, 11.51 mmol) was dissolved in EtOH (50 mL) and the resultant mixture was heated to reflux, whereupon hydrazine hydrate (64%, 1.22 mL, 24.09 mmol) was added and the mixture was stirred at reflux for 3 h. The suspension was then cooled and the resultant precipitate was filtered. The filtrate was evaporated to give a crude oily solid (7 g), which was purified by SiO$_2$ chromatography (9:1, DCM/MeOH with 1% Et$_3$N) to give compound **13** as a crystalline white solid (5.97 g, 94%): ^{1}H NMR (600 MHz, CDCl$_3$) δ 3.13 (s, 2H), 3.25 (s, 3H), 6.92 (d, J = 8.0 Hz, 2H), 7.74 (d, J = 8.0 Hz, 2H); ^{13}C NMR (151 MHz, CDCl$_3$) δ 37.3, 44.1, 93.3, 129.1, 139.1, 142.4, 172.6; IR (ATR) v_{max}/cm^{-1} 3365m, 3301w, 3055w, 2947w, 2885w, 1649s, 1570m, 1486m, 1423m, 1345m, 1109m, 1013m, 892s; MS(ES): m/z = 291.1 [M+H]$^+$; HRMS (ES) calcd. for C$_9$H$_{12}$N$_2$OI [M+H]$^+$: 290.9994, found 291.0012.

N-(2-Aminoethyl)-4-iodo-*N*-methylaniline, 14

Compound **13** (5.72 g, 19.72 mmol) was dissolved in anhydrous toluene (50 mL) under N$_2$, whereupon BH$_3$.Me$_2$S (2.0 M, 10.35 mL, 20.70 mmol) was added and the resultant solution was stirred at reflux for 16 h. The solution was cooled, and 10% Na$_2$CO$_3$ was added, whereupon the solution was stirred vigorously for 10 mins. The solution was then diluted with EtOAc, washed with H$_2$O and brine, dried (MgSO$_4$) and evaporated to give a crude yellow oil (4.4 g). This was purified by SiO$_2$ chromatography (9:1, DCM:MeOH, 0.5% Et$_3$N) to give compound **14** as a yellow oil (3.46 g, 64%), which was carried immediately to the next step: ^{1}H NMR (400 MHz, CDCl$_3$) δ 2.90 (t, J =

6.6 Hz, 2H), 2.93 (s, 3H), 3.36 (t, J = 6.65 Hz, 2H), 6.47 – 6.57 (m, 2H), 7.41 – 7.49 (m, 2H).

Methyl (2*E*)-3-[4-(2-{4-[(2-aminoethyl)(methyl)amino]phenyl}ethynyl)phenyl]prop-2-enoate, 3c

Compound **14** (3.46 g, 12.53 mmol) was dissolved in Et$_3$N (120 mL) and the solution was degassed by sparging with Ar for 1 h. Compound **7a** (2.57 g, 13.8 mmol), Pd(PPh$_3$)$_2$Cl$_2$ (440 mg, 0.63 mmol) and CuI (120 mg, 0.63 mmol) were then added under Ar and the resultant suspension was stirred at 60 °C for 72 h. The solvent was then evaporated to give a crude solid which was purified by SiO$_2$ chromatography (9:1, DCM/MeOH, 0.5% Et$_3$N) to give compound **3c** as a yellow solid (2.44 g, 58%): ^{1}H NMR (600 MHz, DMSO-d_6) δ 2.94 (t, J = 7.0 Hz, 2H), 2.97 (s, 3H), 3.56 (t, J = 7.0 Hz, 2H), 3.73 (s, 3H), 6.67 (d, J = 16.0 Hz, 1H), 6.79 (d, J = 9.0 Hz, 2H), 7.40 (d, J = 8.9 Hz, 2H), 7.47 – 7.54 (m, 2H), 7.67 (d, J = 16.0 Hz, 1H), 7.74 (d, J = 8.3 Hz, 2H); ^{13}C NMR (151 MHz, DMSO-d_6) δ 36.3, 38.1, 49.6, 51.5, 87.4, 93.1, 108.6, 111.9, 118.2, 118.2, 125.1, 128.6, 131.2, 132.7, 133.3, 143.6, 148.9, 166.6; IR (ATR) v_{max}/cm^{-1} 3403br, 3042w, 2952w, 2888w, 2208m, 1698s, 1632m, 1608m, 1594s, 1522s, 1313s, 1169s, 1134s, 817s; MS(ASAP): m/z = 335.2 [M+H]$^+$; HRMS (ASAP) calcd. for C$_{21}$H$_{23}$N$_2$O$_2$[M+H]$^+$: 335.1760, found 335.1743.

Methyl (2*E*)-3-(4-{2-[4-(4-acetylpiperazin-1-yl)phenyl]ethynyl}phenyl)prop-2-enoate, 4a

Compound **3b** (0.35 g, 1.01 mmol) was dissolved in DCM (10 mL), whereupon acetyl chloride (86 µL, 1.21 mmol) and pyridine (98 µL, 1.21 mmol) were added and the resultant solution was stirred at RT for 16 h. The solution was diluted with DCM, washed with sat. NH$_4$Cl and H$_2$O, dried (MgSO$_4$) and evaporated to give a crude yellow solid (0.4 g). This was purified by SiO$_2$ chromatography (97.5:2.5, DCM/MeOH) to give compound **4a** as a yellow solid (0.38 g, 97%): ^{1}H NMR (600 MHz, CDCl$_3$) δ 2.15 (s, 3H), 3.24 (t, J = 5.3 Hz, 2H), 3.27 (t, J = 5.3 Hz, 2H), 3.63 (t, J = 5.2 Hz, 2H), 3.78 (t, J = 5.3 Hz, 2H), 3.81 (s, 3H), 6.44 (d, J = 16.0 Hz, 1H), 6.88 (d, J = 8.4 Hz, 2H), 7.41 – 7.47 (m, 2H), 7.46 – 7.54 (m, 4H), 7.67 (d, J = 16.0 Hz, 1H); ^{13}C NMR (151 MHz, CDCl$_3$) δ 21.3, 41.1, 45.9, 48.3, 48.6, 51.7, 88.0, 92.1, 113.8, 115.6, 118.1, 125.7, 128.0, 131.8, 132.9, 133.7, 144.0, 150.5, 167.3, 169.0; IR (ATR) v_{max}/cm^{-1} 3039w, 2947w, 2836w, 2205w, 2173w, 1699m, 1627s, 1594m, 1521m, 1446m, 1425m, 1311m, 1236s, 1164s, 994s, 835s, 822s; MS(ASAP): m/z = 388.2 [M+H]$^+$; HRMS (ASAP) calcd. for C$_{24}$H$_{24}$N$_2$O$_3$ [M+H]$^+$: 388.1787, found 388.1793.

(3-{4-[4-(2-{4-[(1*E*)-3-methoxy-3-oxoprop-1-en-1-yl]phenyl}ethynyl)phenyl]piperazin-1-yl}propyl)triphenylphosphonium bromide, 5a

Compound **3b** (0.35 g, 1.01 mmol) was dissolved in anhydrous DMF (10 mL) under Ar, whereupon K$_2$CO$_3$ (0.167 g, 1.2 mmol) and (3-bromopropyl)triphenylphosphonium bromide (0.47 g, 1.01 mmol) were added and the resultant solution was stirred at 80 °C for 16 h. The solution was cooled, diluted with H$_2$O and extracted with EtOAc.

The organics were washed with H$_2$O and brine, dried (MgSO$_4$) and evaporated to give a crude yellow solid (0.5 g). This was purified by SiO$_2$ chromatography (95:5, DCM/MeOH) and further recrystallisation from a DCM/heptane solution to give compound **5a** as a yellow solid (0.44 g, 60%): ^{1}H NMR (600 MHz, CDCl$_3$) δ 1.82-1.91 (m, 2H), 2.52-2.58 (m, 4H), 2.74 (t, J = 6.3 Hz, 2H), 3.16-3.23 (m, 4H), 3.79 (s, 3H), 3.91-3.99 (m, 2H), 6.41 (d, J = 16.0 Hz, 1H), 6.77 – 6.84 (m, 2H), 7.32 – 7.42 (m, 2H), 7.39 – 7.52 (m, 4H), 7.64 (d, J = 16.0 Hz, 1H), 7.66-7.73 (m, 6H), 7.75-7.81 (m, 3H), 7.81 – 7.90 (m, 6H); ^{13}C NMR (151 MHz, CDCl$_3$) δ 19.8 (d, J = 3.2 Hz), 20.1 (d, J = 51.8 Hz), 47.9, 51.7, 52.7, 57.1 (d, J = 16.5 Hz), 87.6, 92.5, 112.7, 114.9, 117.9, 118.2, 118.7, 125.8, 127.9, 130.4 (d, J = 12.5 Hz), 131.7, 132.7, 133.4, 133.6 (d, J = 10.0 Hz), 135.0 (d, J = 3.1 Hz), 144.0, 150.8, 167.3; IR (ATR) v_{max}/cm^{-1} 3362br, 2952w, 2876w, 2826w, 2206w, 1703m, 1630m, 1595s, 1519s, 1437s, 1425m, 1324m, 1240s, 1169s, 1111s, 996s, 823s; MS(ES): m/z = 649.4 [M]$^+$; HRMS (ES) calcd. for C$_{43}$H$_{42}$N$_2$O$_2$P [M]$^+$: 649.2984, found 649.2991.

Methyl (2*E*)-3-{4-[2-(4-{methyl[2-(4-methylbenzenesulfonamido)ethyl]amino}phenyl)ethynyl]phenyl}prop-2-enoate, 5b

Compound **3c** (0.35 g, 1.05 mmol) was dissolved in DCM (30 mL), whereupon p-toluenesulfonyl chloride (0.24 g, 1.26 mmol) and Et$_3$N (0.18 mL, 1.26 mmol) were added and the resultant solution was stirred at RT for 16 h. The solution was diluted with DCM, washed with H$_2$O, dried (MgSO$_4$) and evaporated to give a crude yellow solid (0.5 g). This was purified by SiO$_2$ chromatography (99:1, DCM/MeOH) to give compound **5b** as a yellow solid (0.47 g, 92%): ^{1}H NMR (600 MHz, CDCl$_3$) δ 2.42 (s, 3H), 2.92 (s, 3H), 3.15 (q, J = 6.4 Hz, 2H), 3.48 (t, J = 6.4 Hz, 2H), 3.81 (s, 3H), 4.78 (t, J = 6.4 Hz, 1H), 6.43 (d, J = 16.0 Hz, 1H), 6.57 – 6.62 (m, 2H), 7.29 (d, J = 8.1 Hz, 2H), 7.34 – 7.39 (m, 2H), 7.45 – 7.52 (m, 4H), 7.66 (d, J = 16.0 Hz, 1H), 7.70 – 7.74 (m, 2H); ^{13}C NMR (151 MHz, CDCl$_3$) δ 21.5, 38.6, 40.3, 51.7, 52.2, 87.5, 92.8, 110.5, 112.0, 117.9, 126.0, 127.0, 128.0, 129.8, 131.6, 133.0, 133.3, 136.7, 143.6, 144.1, 148.8, 167.4; IR (ATR) v_{max}/cm^{-1} 3241br, 2949w, 2921w, 2857w, 2210m, 1711m, 1632w, 1595s, 1524s, 1320m, 1156s, 1145s, 819s; MS(ASAP): m/z = 489.2 [M+H]$^+$; HRMS (ASAP) calcd. for C$_{28}$H$_{29}$N$_2$O$_4$S [M+H]$^+$: 489.1848, found 489.1866.

General photophysical information
Absorption and Emission Spectra

Absorption and emission spectra were obtained using a CLARIOstar (BMG Labtech) plate reader. For absorption spectra, 100 µM solutions were added to the wells of a UV-transparent 96-well microplate (Corning) and absorbances were recorded at 1 nm intervals. These curves were scaled using extinction coefficient measurements at 400 nm made using a USB4000 spectrometer (OceanOptics) coupled to a xenon white light source, with the dyes held in a 3 mm path length optical cuvette (Hellma). Emission spectra were obtained at 1 nm intervals from 10 µM solutions in microplates using 355 (±5) nm excitation and an 8 nm emission bandwidth.

Quantum Yield Measurement

Quantum yields were measured by applying the reference sample method[37] in a 96-well plate format using the CLARIOstar plate reader. Acridine yellow in ethanol (quantum yield = 0.47[38]) was used as the reference. Seven wells of both reference and sample solutions

were produced by varying the concentration of the dye, aiming for absorbances between 0.01 and 0.07. Across all compounds, these corresponded to concentrations in the 10-100 μM range. The absorbances of each well were recorded between 350-360 nm and the corresponding fluorescence intensity was measured between 380-720 nm. Linear fits of the fluorescence against absorbance datasets were performed for each sample using Origin (Originlab). Quantum yields were obtained by dividing the gradient of the sample data by the gradient of the reference data, correcting for solvent refractive index using literature values.[39]

Fluorescence Lifetimes

Fluorescence decay measurements were performed as previously[40] using an Ortec modular time-correlated single photon counting (TCSPC) system. 250 kHz pulsed excitation at 350 nm was obtained by using a barium borate (BBO) crystal to frequency double the 700 nm output of an optical parametric amplifier pumped by a Ti:sapphire regenerative amplifier system (all Coherent). Emission events were collected for 10 minutes through 435-650 nm emission filtering. Multiexponential decay fitting was performed in Origin (Originlab), with χ_R^2 values averaging 1.6 (±0.4) across all measurements.

pH versus fluorescence

Buffer solutions at pH 5 (0.1 M NaOAc), pH 7.5 (0.01 M phosphate buffer, 0.027 M KCl, 0.137 M NaCl) and pH 9 (0.1 M sodium borate) were freshly prepared and the pH was measured immediately before the experiment (final pH values: 5.01, 7.50 and 9.01, respectively). Compound solutions in each buffer were prepared by dilution from a freshly prepared 10 μM stock solution in DMSO, to a concentration of 326 nM (3.3% *v/v* DMSO). The solutions of each compound were analysed in quartz cuvettes using a Varian Cary Eclipse Fluorescence Spectrophotometer by recording the fluorescence spectrum between 400-700 nm with excitation at 360 nm, with an excitation slit width of 5 nm and an emission slit width of 10 nm. The background fluorescence from the buffer solutions was subtracted to give the fluorescence spectra of each compound at pH 5, 7.5 and 9.

General biological information
Cells

HaCaT human epidermal keratinocytes were purchased from a commercial supplier (Thermo Fisher) and the cell line was cultured at 37 °C/5% CO$_2$ in DMEM (Gibco cat. no. 10566, high glucose, GlutaMAX supplement) with 10% foetal calf serum and 1% penicillin/streptomycin. For experiments, cells were plated in 8-well chambered coverslips at concentrations between 2.5×10^4 to 10.0×10^4 cells per mL. Cells were treated for 30 min with 1 μM concentrations (unless otherwise stated) of compounds **1a**-**5b** (from 10 mM stock solutions in DMSO) in media. For all experiments a minimum of three repeats were taken.

Imaging

Cells were imaged using either a Zeiss 880 Laser Scanning Confocal Microscope (LSCM) with Airyscan detection or a Leica SP5 LSCM. Live cells were imaged inside an environmental chamber at 37 °C and 5% CO$_2$. Samples were fixed by treatment with paraformaldehyde/PBS (PFA, 4%) for 20 min at RT. Samples imaged on the Zeiss 880 microscope were excited with a 405 nm, 488 nm, 594 nm or 633 nm laser and imaged with a Plan-Apochromat Leica 63x 1.2NA HCX PL APO Oil UV long working distance objective lens.

Colocalisation

Cells plated on 8-well chambered plates were co-stained with compounds **1a-5b** and live cell markers for various organelles for 30 min and then washed twice with PBS. PBS was added to each well for imaging purposes. Co-localisation analysis was conducted using the ImageJ tool Coloc2, in which the background was subtracted, and an ROI was selected in each case. The Zeiss 880 microscope was used for this work.

MitoTracker® Red

Cells were co-stained with compounds 1a-5b and 200 nM MitoTracker® Red (ThermoFisher, cat. no. M22425) in media for 30 min, then rinsed twice with PBS (pH 7.2). MitoTracker was excited using a 633 nm laser.

Nile Red

Cells were co-stained with compounds **1a-5b** and 10 μg/mL Nile Red (Fisher Scientific, cat. no. 11549116) in media for 30 min, then rinsed twice with PBS (pH 7.2). Nile Red was excited using a 594 nm laser.

BODIPY™ 493/503

Cells were co-stained with compounds **1a-5b** and 2 μM BODIPY™ 493/503 (Fisher Scientific, cat. no. D3922) in media for 30 min, then rinsed twice with PBS (pH 7.2). BODIPY™ 493/503 was excited using a 488 nm laser.

LysoTracker™ Red DND-99

Cells were co-stained with compounds **1a-5b** and 50 nM LysoTracker™ Red DND-99 (Fisher Scientific, cat. no. 12090146) in media for 30 min, then rinsed twice with PBS (pH 7.2). LysoTracker™ Red DND-99 was excited using a 594 nm laser.

BODIPY™ ER-Tracker™ Red

Cells were co-stained with compounds **1a-5b** and 1 μM BODIPY™ ER-Tracker™ Red (Fisher Scientific, cat. no. 11584746) in media for 30 min, then rinsed twice with PBS (pH 7.2). BODIPY™ ER-Tracker™ Red was excited using a 594 nm laser.

Relative Intensity

Cells plated in 8-well plates were treated with compounds **1a-5b** (1 μM) and fixed with PFA. The samples were imaged using a 405 nm laser at 0.2% and the detector was set to the range of 415-735 nm and a gain of 500. The pinhole was set to 4.88 Airy units to maximise the amount of light collected. Using ImageJ for the analysis, thresholding at a low tolerance level was used to select the cells in the images, removing any background areas devoid of cells. The normalised average intensity per pixel was

used as the comparison metric between the compounds. The Zeiss 880 microscope was used for this work.

Lambda Scans

Three lambda scans were performed for each compound - each on different cell samples. To reduce noise, each sample had the line averaging set to 2, however there was no frame averaging. The three scans were processed in ImageJ by taking the intensity at each frame (wavelength step) and then averaging. To further account for photobleaching, snapshots were taken before and after each lambda scan with a detector range of 415-735 nm. The intensity of the snapshots was measured using ImageJ and fit to an inverse exponential model by using the solver function in Microsoft Excel to perform least squares analysis. The lambda scan data was adjusted accordingly. The Zeiss 880 microscope was used for this work.

Photostability

Cells plated in 8 well-plates were stained with 5 µM of compounds **1a**, **1b** & **4a** and 1 µM for the rest of the compounds for 30 min. Live and fixed samples were used in this experiment. The samples were imaged at 10% power and the detector was set to a gain of 700. 100 data points were taken, and ImageJ was used to calculate the average pixel intensity of each frame. The resultant data was fit to an inverse mono-exponential model using the solver function in Microsoft Excel to perform least squares analysis. The half-life (number of frames taken to reach half the initial intensity) was calculated and used as the measure of comparison. The Leica Sp5 microscope was used for this work.

Conflicts of interest

A. W. and C. A. A. are LightOx Limited shareholders, the company licensed to pursue commercial applications of the novel compounds described in this manuscript.

Acknowledgements

Notes and references

1   H. Kobayashi, M. Ogawa, R. Alford, P. L. Choyke and Y. Urano, *Chem. Rev.*, 2010, **110**, 2620–2640.

2   Y. Fu and N. S. Finney, *RSC Adv.*, 2018, **8**, 29051–29061.

3   I. Sarkar and A. K. Mishra, *Appl. Spectrosc. Rev.*, 2018, **53**, 552–601.

4   E. A. Specht, E. Braselmann and A. E. Palmer, *Annu. Rev. Physiol.*, 2017, **79**, 93–117.

5   E. Kim, Y. Lee, S. Lee and S. B. Park, *Acc. Chem. Res.*, 2015, **48**, 538–547.

6   J. B. Grimm, B. P. English, J. Chen, J. P. Slaughter, Z. Zhang, A. Revyakin, R. Patel, J. J. Macklin, D. Normanno, R. H. Singer, T. Lionnet and L. D. Lavis, *Nat. Methods*, 2015, **12**, 244–250.

7   L. D. Hughes, R. J. Rawle and S. G. Boxer, *PLoS One*, 2014, **9**, 1–8.

8   L. C. Zanetti-Domingues, C. J. Tynan, D. J. Rolfe, D. T. Clarke and M. Martin-Fernandez, *PLoS One*, , DOI:10.1371/journal.pone.0074200.

9   S. H. Alamudi, R. Satapathy, J. Kim, D. Su, H. Ren, R. Das, L. Hu, E. Alvarado-Martínez, J. Y. Lee, C. Hoppmann, E. Penã-Cabrera, H. H. Ha, H. S. Park, L. Wang and Y. T. Chang, *Nat. Commun.*, 2016, **7**, 11964.

10   P. Gao, W. Pan, N. Li and B. Tang, *Chem. Sci.*, 2019, **10**, 6035–6071.

11   N. Zheng, H. N. Tsai, X. Zhang and G. R. Rosania, *Mol. Pharm.*, 2011, **8**, 1619–1628.

12   X. Chen, M. Velliste and R. F. Murphy, *Cytom. A*, 2006, **69**, 631–640.

13   G. R. Rosania, K. Shedden, N. Zheng and X. Zhang, *J. Cheminform.*, 2013, **5**, 44.

14   R. W. Horobin, F. Rashid-Doubell, J. D. Pediani and G. Milligan, *Biotech. Histochem.*, 2013, **88**, 440–460.

15   K. W. Dunn, M. M. Kamocka and J. H. McDonald, *Am. J. Physiol. Cell Physiol.*, 2011, **300**, C723–C742.

16   D. R. Chisholm, R. Lamb, T. Pallett, V. Affleck, C. Holden, J. Marrison, P. O'Toole, P. D. Ashton, K. Newling, A. Steffen, A. K. Nelson, C. Mahler, R. Valentine, T. S. Blacker, A. J. Bain, J. M. Girkin, T. B. Marder, A. Whiting and C. A. Ambler, *Chem. Sci.*, 2019, **10**, 4673–4683.

17   J. Gala De Pablo, D. R. Chisholm, A. Steffen, A. K. Nelson, C. Mahler, T. B. Marder, S. A. Peyman, J. M. Girkin, C. A. Ambler, A. Whiting and S. D. Evans, *Analyst*, 2018, **143**, 6113–6120.

18   J. R. Casey, S. Grinstein and J. Orlowski, *Nat. Rev. Mol. Cell Biol.*, 2010, **11**, 50–61.

19   D. R. Chisholm, C. W. E. Tomlinson, G.-L. Zhou, C. Holden, V. Affleck, R. Lamb, K. Newling, P. Ashton, R. Valentine, C. Redfern, J. Erostyák, G. Makkai, C. A. Ambler, A. Whiting and E. Pohl, *ACS Chem. Biol.*, 2019, **14**, 369–377.

20   D. R. Chisholm, G.-L. Zhou, E. Pohl, R. Valentine and A. Whiting, *Beilstein J. Org. Chem.*, 2016, **12**, 1851–1862.

21   R. A. J. Smith, C. M. Porteous, A. M. Gane and M. P. Murphy, *Proc. Natl. Acad. Sci. USA*, 2003, **100**, 5407–5412.

22   J. Zielonka, J. Joseph, A. Sikora, M. Hardy, O. Ouari, J. Vasquez-Vivar, G. Cheng, M. Lopez and B. Kalyanaraman, *Chem. Rev.*, 2017, **117**, 10043–10120.

23   R. Chawla, V. Van Puyenbroeck, N. C. Pflug, A. Sama, R. Ali, D. Schols, K. Vermeire and T. W. Bell, *J. Med. Chem.*, 2016, **59**, 2633–2647.

24   H. Xiao, C. Wu, P. Li, W. Gao, W. Zhang, W. Zhang, L. Tong and B. Tang, *Chem. Sci.*, 2017, **8**, 7025–7030.

25   C. Dehu, F. Meyers and J. L. Bredas, *J. Am. Chem. Soc.*, 1993, **115**, 6198–6206.

26   Z. Diwu, Y. Lu, C. Zhang, D. H. Klaubert and R. P. Haugland, *Photochem. Photobiol.*, 1997, **66**, 424–431.

27   G. M. Cooper, *The Cell: A Molecular Approach*, Sinauer Associates, Sunderland (MA), 2nd edn., 2000.

28   P. Greenspan, E. P. Mayer and S. D. Fowler, *J. Cell Biol.*, 1985, **100**, 965–973.

29   X. Chen, Y. Bi, T. Wang, P. Li, X. Yan, S. Hou, C. E. Bammert,

J. Ju, K. M. Gibson, W. J. Pavan and L. Bi, *Sci. Rep.*, 2015, **5**, 9004.

30   ACD/I-Lab 2.0, Advanced Chemistry Development Inc., Toronto, ON, Canada, www.acdlabs.com, 2020.

31   H. Zhang, J. Chen, H. Xiong, Y. Zhang, W. Chen, J. Sheng and X. Song, *Org. Biomol. Chem.*, 2019, **17**, 1436–1441.

32   S. Xu, H. W. Liu, X. X. Hu, S. Y. Huan, J. Zhang, Y. C. Liu, L. Yuan, F. L. Qu, X. B. Zhang and W. Tan, *Anal. Chem.*, 2017, **89**, 7641–7648.

33   B. K. McMahon, R. Pal and D. Parker, *Chem. Commun.*, 2013, **49**, 5363–5365.

34   S. Singha, D. Kim, B. Roy, S. Sambasivan, H. Moon, A. S. Rao, J. Y. Kim, T. Joo, J. W. Park, Y. M. Rhee, T. Wang, K. H. Kim, Y. H. Shin, J. Jung and K. H. Ahn, *Chem. Sci.*, 2015, **6**, 4335–4342.

35   G. Cristalli, E. Camaioni, S. Vittori, R. Volpini, P. A. Borea, A. Conti, S. Dionisotti, E. Ongini and A. Monopoli, *J. Med. Chem.*, 1995, **38**, 1462–1472.

36   G. Modi, T. Antonio, M. Reith and A. Dutta, *J. Med. Chem.*, 2014, **57**, 1557–1572.

37   A. T. Rhys Williams, S. A. Winfield and J. N. Miller, *Analyst*, 1983, **108**, 1067–1071.

38   J. Olmsted, *J. Phys. Chem.*, 1979, **83**, 2581–2584.

39   I. Z. Kozma, P. Krok and E. Riedle, *J. Opt. Soc. Am. B*, 2005, **22**, 1479–1485.

40   T. S. Blacker, N. Nicolaou, M. R. Duchen and A. J. Bain, *J. Phys. Chem. B*, 2019, **123**, 4705–4717.